April 12, 2011 | vol. 108 | no. 15 | pp. 5954–5963

PNAS

Proceedings of the National Academy of Sciences of the United States of America www.pnas.org

An RNAi-based chemical genetic screen identifies three small-molecule inhibitors of the Wnt/*wingless* signaling pathway

Foster C. Gonsalves, Keren Klein, Brittany B. Carson, Shauna Katz, Laura A. Ekas, Steve Evans, Robert Nagourney, Timothy Cardozo, Anthony M. C. Brown, and Ramanuj DasGupta

An RNAi-based chemical genetic screen identifies three small-molecule inhibitors of the Wnt/*wingless* signaling pathway

Foster C. Gonsalves[a,b], Keren Klein[a], Brittany B. Carson[c], Shauna Katz[a,b], Laura A. Ekas[a,b], Steve Evans[d], Robert Nagourney[d], Timothy Cardozo[a], Anthony M. C. Brown[c], and Ramanuj DasGupta[a,b,1]

[a]Department of Pharmacology and [b]New York University Cancer Institute, New York University Langone Medical Center, New York, NY 10016; [c]Department of Cell and Developmental Biology, Weill Cornell Medical College, New York, NY 10065; and [d]Rational Therapeutics, Long Beach, CA 90806

This Feature Article is part of a series identified by the Editorial Board as reporting findings of exceptional significance.

Edited by Elaine Fuchs, The Rockefeller University, New York, NY, and approved February 11, 2011 (received for review November 26, 2010)

Misregulated β-catenin responsive transcription (CRT) has been implicated in the genesis of various malignancies, including colorectal carcinomas, and it is a key therapeutic target in combating various cancers. Despite significant effort, successful clinical implementation of CRT inhibitory therapeutics remains a challenging goal. This is, in part, because of the challenge of identifying inhibitory compounds that specifically modulate the nuclear transcriptional activity of β-catenin while not affecting its cytoskeletal function in stabilizing adherens junctions at the cell membrane. Here, we report an RNAi-based modifier screening strategy for the identification of CRT inhibitors. Our data provide support for the specificity of these inhibitory compounds in antagonizing the transcriptional function of nuclear β-catenin. We show that these inhibitors efficiently block Wnt/β-catenin–induced target genes and phenotypes in various mammalian and cancer cell lines. Importantly, these Wnt inhibitors are specifically cytotoxic to human colon tumor biopsy cultures as well as colon cancer cell lines that exhibit deregulated Wnt signaling.

high-throughput screen | oxazole | thiazole | thiazolidinedione | beta-catenin

Wnt genes encode secreted glycoproteins that belong to a family of conserved signaling molecules which regulate a plethora of fundamental developmental and cell biological processes (1–3). Aberrant or sustained Wnt signaling has been linked to human disease, including cancers of the liver, colon, breast, and skin (2, 4–6). The key mediator of canonical Wnt signaling is the transcriptional coactivator β-catenin (β-cat). The cytosolic level of β-cat is tightly controlled by a multiprotein destruction complex composed of Adenomatous polyposis coli (APC), Axin, and Glycogen synthase kinase-3β (GSK-3β), which phosphorylates β-cat and thereby, induces its ubiquitination and subsequent proteasome-mediated degradation (Fig. 1*A*) (7–10). Stimulation of the pathway by Wnts results in inhibition of the destruction complex, leading to stabilization/activation of cytosolic β-cat, which translocates to the nucleus and activates transcription together with the Lymphoid enhancer factor/T-cell factor (LEF/TCF) family of transcription factors (1, 11–13). Thus, catenin responsive transcription (CRT), which corresponds to the activation program of transcriptional targets of β-cat, is a critical aspect of the responsiveness of a cell to a specific Wnt stimulus. Most, if not all, Wnt-associated carcinogenesis results from misregulated CRT, thus making the β-cat-TCF4 complex an ideal therapeutic target for drug design (14–19).

Significant effort and resources have been invested in the identification of small-molecule prototypes capable of regulating CRT (20–24). Some of these compounds were identified in cell-free assays, thus risking limited use of the compounds in cellular environments (20). Other compounds, such as ICG-001, which block CRT by interfering with the ability of β-cat to bind CREB protein (CBP), raise possible concerns regarding specificity, because CBP is known to interact with numerous other transcription factors, thereby influencing many signaling pathways (23). More recent efforts to identify Wnt signaling modulators have resulted in candidate compounds that inhibit Wnt signaling by influencing the stability and expression levels of β-cat (21, 22, 24). Although the use of such compounds in inhibiting the transcriptional activity of β-cat can be easily envisioned, there is a significant risk that they may also perturb the function of β-cat in cell–cell adhesive junctions (25, 26). Such down-regulation of β-cat–dependent adherens junctions is often associated with the initial stages of tumor metastasis. Moreover, treatment with compounds reducing β-cat expression might prove deleterious to the overall structural integrity and viability of cells, resulting in undesired systemic effects in vivo.

Compounds that inhibit aspects of Wnt signaling upstream of the axin/APC/GSK-3β complex, such as secretion or reception of Wnt ligands at the plasma membrane (21, 27) or transduction of the Wnt signal by Dishevelled (Dvl) (27, 28), could also result in cross-regulatory effects on other signaling events activated by Wnts. These include the non-canonical pathways that lead to PKC and JNK activation, resulting in calcium release and cytoskeletal rearrangements (1). Moreover, therapeutic applicability of such compounds is limited in cases where the Wnt pathway is deregulated by mutations in downstream components of the pathway, such as Axin, APC, or β-cat. Finally, several of the enzymatic components of the Wnt cascade that could potentially serve as attractive targets for small molecules, such as GSK-3β, caesin kinase 1 alpha (CK1α), and beta-transducin repeat containing protein (β-TrCP), also modulate other signaling pathways, thereby diminishing their suitability as Wnt-specific therapeutic targets (24, 29).

We reasoned that, for the purpose of developing CRT-inhibitory drugs, it would be ideal to identify compounds that can uncouple the function of β-cat in the nucleus from that at the plasma membrane. Our goal was to identify small molecules that would target CRT without promoting indiscriminate degradation of β-cat or inhibiting its interaction with E-cadherin (E-cad) and other junction proteins (30–33). We devised a highly targeted suppressor screen that incorporates advantages of RNAi technology so as to specifically modulate the activity of the β-cat-TCF

Author contributions: F.C.G., S.E., R.N., T.C., A.B., and R.D. designed research; F.C.G., K.K., B.C., S.K., L.A.E., S.E., and R.D. performed research; F.C.G., K.K., B.C., L.A.E., S.E., R.N., T.C., A.B., and R.D. analyzed data; and F.C.G. and R.D. wrote the paper.

The authors declare no conflict of interest.

This article is a PNAS Direct Submission.

Freely available online through the PNAS open access option.

See Commentary on page 5929.

[1]To whom correspondence should be addressed. E-mail: ramanuj.dasgupta@nyumc.org.

This article contains supporting information online at www.pnas.org/lookup/suppl/doi:10.1073/pnas.1017496108/-/DCSupplemental.

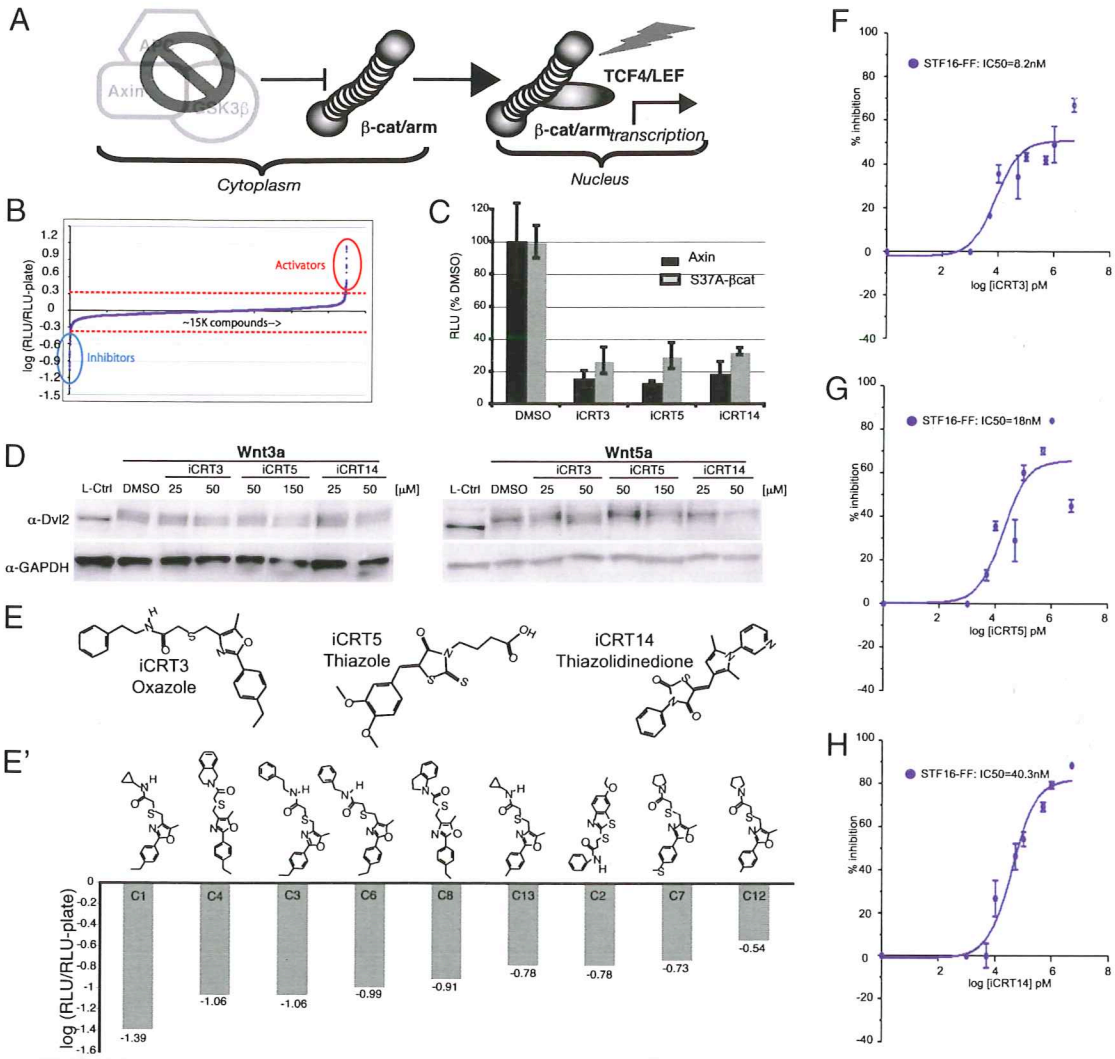

Fig. 1. (*A*) Primary screen. dsRNA-mediated knockdown of Axin results in cytoplasmic stabilization of β-cat, which, on translocation to the nucleus, results in activation of the β-cat responsive dTF12 reporter. (*B*) dTF12-luciferase activity in response to treatments with a small-molecule library, normalized to plate average, shows that, for all compounds screened, most had little or no effect on Wg signaling. Cut-off for cherry picking lead hits was set at ±0.3 on a logarithmic scale (red dashed line), reflecting either a twofold activation (red oval) or reduction (blue oval). The *x* axis represents the compounds screened, and the *y* axis represents the log transformation of the fold change of the dTF12 reporter for individual compounds over that of the plate average. (*C*) Reporter activity in Cl8 cells transfected with degradation-resistant β-cat is inhibited by candidate inhibitors to a similar extent as in cells transfected with dAxin dsRNA. (*D*) Western analysis of Dvl2 phosphorylation in Rat2 cells pretreated with iCRTs at the indicated doses and stimulated for 2 h with Wnt3a (*Left*) or Wnt5a (*Right*). The upper band, where present, is the phosphorylated form induced by noncanonical Wnt signaling. (*E*) Candidate inhibitors identified in the primary screen fall into three families: Oxazoles, Thiazoles, and Thiazolidinedione. (*E'*) Compounds belonging to the Oxazole family (like iCRT3 or C3), which were identified, in the primary screen as strong hits. The majority of them were also tested in secondary specificity and epistasis assays (Fig. S1 *B* and *C*). (*F–H*) Dose-response analysis of the Wnt responsive STF16-luc reporter in the presence of varying concentrations of iCRT3 (*F*), -5 (*G*), and -14 (*H*) in mammalian HEK293 cells.

transcriptional complex downstream of the axin-mediated degradation complex. The initial assay used the Wnt responsive luciferase reporter-dTF12 in *Drosophila* clone 8 (Cl8) cells, as previously described (34). Use of *Drosophila* cells for the primary screen provided a robust assay in the absence of genetic redundancies present in the mammalian system. Wnt/β-cat signaling was activated by introducing dsRNAs specific for axin (Fig. 1*A*), and we then assessed the effect of individual compounds from a small-molecule library on the resulting induction of dTF12 reporter activity. This allowed us to selectively target the Wnt cascade downstream of the destruction complex and avoid compounds that might interfere with pathway components farther upstream (Fig. 1*A*). We therefore anticipated that the candidate compounds identified using this approach would affect the activated or stable pool of β-cat and modulate its interaction with proteins that mediate the nuclear function of β-cat (35–37). Such compounds would have the advantages of being able to block activated CRT resulting from oncogenic mutations in β-cat itself and nuclear β-cat activity in tumors in which components of the degradation complex are compromised by mutation.

Results

Primary Screen. As proof of concept, we first confirmed that the dTF12 luciferase reporter was strongly activated on dsRNA-mediated knockdown of dAxin (Fig. S1*A*). Importantly, co-knockdown of β-cat (*arm*) or dTCF (*pan*) along with dAxin markedly reduced the reporter activity, consistent with an absolute requirement of β-cat and dTCF to activate target genes downstream of dAxin (Fig. S1*A*). The primary screen was thus designed to identify candidate small molecules that would phenocopy the loss of function of downstream modulators, such as β-cat or dTCF, in the absence of dAxin. The *Z* factor for the

assay was determined to be 0.77, thereby indicating a robust assay system for a high-throughput screen (HTS) (Fig. S1*A* and *SI Materials and Methods* have a detailed description of *Z* factor).

We screened 14,977 compounds from small-molecule libraries in the Institute of Chemistry and Cellular Biology (ICCB)–Longwood collection (ICCB, Harvard Medical School, Boston) for their effect on modulation of dAxin-dsRNA–induced dTF12 reporter activity/CRT in *Drosophila* Cl8 cells (Fig. 1 *B* and *C*). The screen was performed in high-throughput format in 384-well microtiter plates. The libraries included known bioactive compounds [National Institute of Neurological Disorders and Stroke (NINDS) custom collection, Specplus, and BIOMOL1 (www.biomol.com, Catalogue #2840)], fungal extracts comprising of a mixture of natural compounds (ICCB), and 10,752 molecules from the ChemDiv3 synthetic library, which is a large collection of low molecular weight and structurally diverse families/classes of compounds.

The primary screen identified 34 molecules that had a statistically significant inhibitory effect on the activity of the dTF12-luciferase reporter gene (total hit rate ~0.3%) (Fig. 1*B*, blue oval). We call these compounds inhibitors of CRT (iCRT). The addition of these compounds to the cells strongly repressed the dTF12 reporter activity by >70% (Fig. 1*B* and Fig. S1). The known chemical structures of these iCRTs suggested that the most potent (iCRT3) belongs to the oxazole class of small molecules (Fig. 1*E*). Interestingly, we identified nine oxazoles as potent inhibitors of the dTF12 reporter activity (Fig. 1*E′*), which may suggest a shared mechanism and/or putative target for this class of iCRTs. The other lead inhibitors belong to the closely related thiazole (iCRT5) or thiazolidinedione (iCRT14) classes (Fig. 1*E*). Thiazolidinediones have recently been reported to down-regulate Wnt/β-cat signaling in breast and prostate cancer cells (38, 39). Importantly, none of the iCRTs, including iCRT3, -5, and -14 (Fig. S1*A′*), influenced the transcriptional activity of FOP-Flash luciferase reporter, which harbors mutations in the DNA binding sites for TCF (β-cat response element), showing specificity of the response. We also isolated eight compounds that significantly and reproducibly activated Wnt pathway activity as measured by the dTF12-luciferase reporter (Fig. 1*B*, red oval). However, this study focuses on the candidate inhibitors (iCRTs) because of their potential relevance to cancer therapy.

Secondary Screens. ***Epistasis analysis in* Drosophila *cells.*** To define the site of action of candidate iCRTs within the Wnt signaling cascade, we designed a series of cell-based epistasis assays. Several proteins, including CK1α, Slimb/βTrcp, and SkpA, are known to regulate the Wnt signaling cascade parallel to or downstream of dAxin. Each of these negatively regulates CRT, either by phosphorylation of β-cat or mediating its subsequent degradation through the ubiquitin–proteosome pathway (7–10). To test the epistatic relationship between the candidate compounds and these known regulators of the pathway, we first activated the Wnt pathway in Cl8 cells using dsRNA targeted to the negative regulator Slimb/βTrCP, which functions downstream of the Axin/APC/GSK-3β complex, and assayed the effect of the iCRTs on dTF12 reporter activity in these cells. We were able to obtain 23 of 31 candidate inhibitors from commercial sources for this secondary analysis; of these, 21 compounds inhibited dTF12 reporter activity downstream of Slimb/βTrCP (Fig. S1*B*). To gain further evidence that the compounds exert their inhibitory effect in the nucleus, we also tested them in Cl8 cells transfected with a construct encoding a degradation-resistant form of β-cat, S37Aβ-cat (Fig. 1*C* and Fig. S1*B*) (40). As shown in Fig. 1*C*, the representative candidate compounds iCRT3, -5, and -14 strongly inhibited S37Aβ-cat–induced dTF12 activity to a similar extent as observed in response to dAxin knockdown. The inhibitory effect of the compounds on the activity of S37Aβ-cat provided further evidence that they exert their effect on Wnt responsiveness at the level of CRT in the nucleus and that the inhibition is independent of levels or nuclear accumulation of β-cat. IC_{50} of most of the candidate inhibitors for the luciferase reporter assay was found to lie in the nanomolar to micromolar range (Table S1), consistent with high potency for inhibiting the Wnt signaling pathway.

Pathway and species specificity of candidate iCRTs. We next tested whether the inhibitory action of the candidate compounds identified in the primary screen was specific to CRT by assaying their effects on other conserved cell signaling pathways. First, we asked if the iCRTs modulate β-cat–independent noncanonical Wnt signaling. For this, we assayed their effect on phosphorylation of Dvl induced by either Wnt3a or Wnt5a because, in each case, this is mediated independently of canonical Wnt signals (41). As shown in Fig. 1*D*, we observed no effect of iCRTs on Wnt-mediated Dvl phosphorylation, with the exceptions that, at higher doses, iCRT3 led to partial inhibition of phosphorylation induced by Wnt5a and iCRT14 showed a modest reduction in the amount of Dvl but had no effect on Dvl phosphorylation itself. These data indicate that, at the lower doses, which are sufficient to antagonize canonical Wnt-mediated CRT, the inhibitors did not prevent noncanonical Wnt signaling through Dvl.

We next monitored the activity of Patched luciferase (Ptc-luc) and STAT-luciferase (STAT-luc) (29, 42) as readouts for the *Hedgehog* (*hh*) and Janus kinase/STAT signaling pathways, respectively, in *Drosophila* cells and CSL luciferase (CSL-luc) as a reporter for Notch signaling pathway in mammalian HEK293 cells (Fig. S1 *C–I*). Although iCRT3 and -5 were up to 1,000 times more potent in inhibiting the mammalian Wnt responsive STF16 luciferase (STF16-luc) reporter in HEK293 cells compared with the Notch responsive CSL luciferase (CSL-luc) reporter (Fig. 1 *F* and *H* and Fig. S1 *D* and *E*), iCRT14 was approximately two times as potent against STF16-luc as against CSL-luc as judged by their respective IC_{50} values (Fig. 1 and Fig. S1*F*). Additionally, in *Drosophila* cells, iCRT3, -5, and -14 were 3–10 times more efficient in inhibiting the Wg responsive dTF12 reporter compared with their effect on Ptc-luc and STAT-luc reporters (Fig. S1 *G–I*). Finally, some of the candidate iCRTs, such as iCRT4, -9, -16, and -21, robustly modulated the other signaling pathway reporters and therefore were discarded from further analysis here (Fig. S1*C*). Taken together, these results indicated that at least some of the candidate inhibitors isolated in the *Drosophila* cell screen also robustly and specifically suppressed CRT in mammalian cells.

Modulation of β-Cat-TCF Complex by Candidate Inhibitors/iCRTs. ***Molecular regulation of β-cat-TCF protein complexes by candidate iCRTs.*** To test whether the lead iCRTs compromised the integrity of β-cat-TCF4 complexes, we preincubated purified recombinant His-tagged β-cat with candidate inhibitors at different concentrations and assayed its ability to bind a purified GST-tagged TCF4 N-terminal domain. This domain of TCF4 has previously been shown to be sufficient for formation of β-cat-TCF4 complexes (43, 44). iCRT3, -5, and -14 noticeably reduced the efficiency of inhibitor-treated β-cat to bind the N-terminal domain of TCF4 (Fig. 2*A*). We next performed coimmunoprecipitation (coIP) assays to examine whether the iCRTs could disrupt endogenous β-cat-TCF complexes in a cellular context. As shown in Fig. 2*B*, treatment of S37Aβ-cat–transfected HEK293 cells, with increasing concentrations of iCRT3, -5, and -14, significantly inhibited β-cat-TCF interactions. This suggests that all three lead compounds are CRT inhibitors that function by inhibiting direct interactions between β-cat and TCF4. When normalized for input and loading, at concentrations that are sufficient to inhibit β-cat-TCF4 interactions, the iCRTs had minimal or no effect on β-cat-E-cad (Fig. 2 *A* and *B*) or β-cat-α-cat interactions (Fig. S2*A*), suggesting that these compounds do not influence β-cat's interactions with other cognate protein partners indiscriminately. CoIP assays of nuclear extracts prepared from *Drosophila* Cl8 cells treated with Axin dsRNA also showed a significant reduction

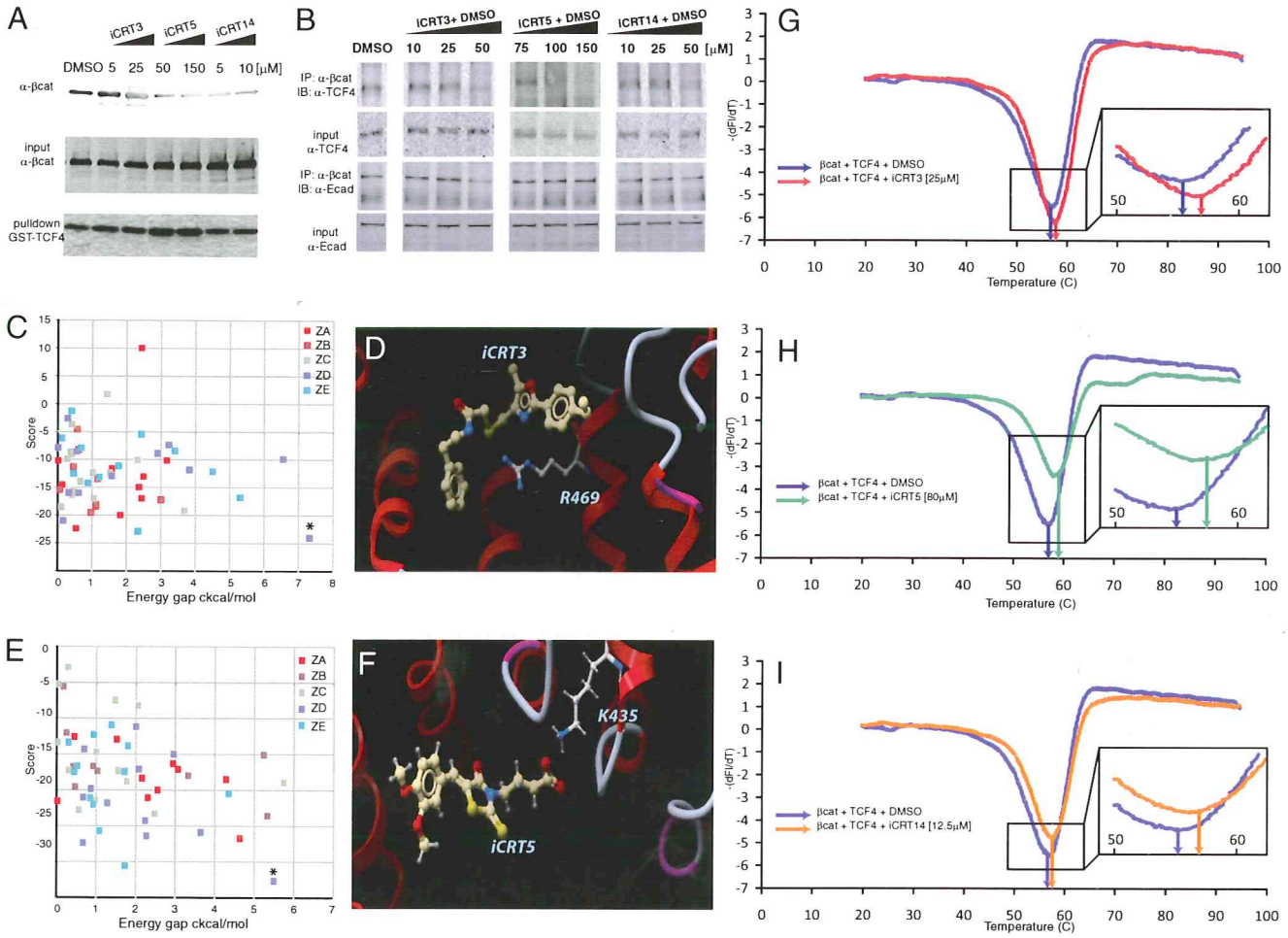

Fig. 2. (*A*) Effect of candidate compounds on the interaction of purified β-cat-His and GST-TCF4. iCRT3, -5, and -14 show a significant inhibitory effect on these interactions compared with nontreated (NT) and DMSO-treated binding reactions. *Bottom* shows comparable amounts of GST-TCF4 being pulled down. (*B*) Effect of candidate compounds on β-cat's interaction with endogenous TCF4. HEK293 cells were transfected with S37Aβ-cat and treated overnight with candidate compounds at the indicated concentrations. β-cat immunoprecipitates from whole-cell lysates blotted for endogenous TCF4 show significant reduction in β-cat-TCF4 interaction in the presence of compounds while having negligible effect on β-cat-E-cad interaction. Images are representative of independent experiments and are from different gels. (*C* and *E*) Colored squares represent the energy scores (*y* axis) of the best alternative conformations that were accepted during the flexible Monte Carlo docking simulation for iCRT3 (*C*) and -5 (*E*) against each of the 20 pockets on the different crystal structures of β-cat (different colors for different Protein Data Bank crystal structures). Asterisk represents the docked conformation with the best energy score, which for these two compounds, is the lowest energy and is clearly distinguishable (significant energy gap; *x* axis) from nearby conformations. (*D* and *F*) Docked conformations of iCRT3 (*D*) and -5 (*F*) in the pocket lined by R469 and K435 on β-cat. (*G–I*) Traces showing negative derivatives of changes in fluorescence of β-cat-TCF4-SYPRO Orange complex in the presence of indicated concentrations of iCRT3 (red trace in *G*), -5 (green trace in *H*), or -14 (orange trace in *I*). Note the shift in the melting temperature (Tm indicated by arrows; *G Inset*, *H Inset*, and *I Inset*) in presence of iCRTs compared with that in the presence of DMSO (blue trace in *G–I*).

in the amount of TCF4 interacting with endogenous β-cat in the presence of the inhibitors (Fig. S2*B*).

Modulation of DNA binding of TCF by iCRTs. Next, we wanted to explore whether candidate iCRTs modulate the STF16 luciferase activity by impacting TCF binding to DNA. We used TCF fusion contructs, ΔβBD-TCF-VP16 and ΔNLEF-β-cat, that can robustly activate the Wnt reporter independent of TCF-β-cat interaction but are dependent on the inherent ability of TCFs to bind DNA. As shown in Fig. S2 *C* and *D*, whereas iCRT3 and -5 had no significant effect on the reporter activated by either ΔβBD-TCF-VP16 or ΔNLEF-β-cat, iCRT14 reduced the STF16 response by ~50%. These results suggest that iCRT14 can also interfere with TCF binding to DNA in addition to its ability to influence TCF-β-cat interaction.

In silico docking of iCRTs onto the co-crystal structure of β-cat/Tcf. To seek evidence of structural complementarities between the inhibitors and the β-cat protein surface, we performed in silico docking analysis based on the β-cat crystal structure. A similar computational approach was recently used by Shan et al. (28), who used structure-based virtual ligand screening (VLS) of a small-molecule library to identify a compound that can specifically bind the PDZ domain of Dvl protein (28).

Distinct residues have been shown to be structurally, functionally, and energetically important for the interaction of β-cat with its different protein partners (44–46). For example, Lys312 and Lys345 on β-cat form specific electrostatic contacts with Glu16 on TCF, whereas Lys435 pairs with Asp16 on TCF, and Phe253 and Phe293 together bury a specific hydrophobic surface with Leu48 on TCF (45–49). Furthermore, mutations in Lys312 and Lys435 have been shown to attenuate the ability of β-cat to activate transcription of the luciferase reporter TOPFlash (50). We anticipated that the lead iCRTs might bind to one or more of these areas and thereby be able to interfere with β-cat-TCF interactions specifically. In silico analyses of the co-crystal structure of β-cat-TCF4 revealed that there are ~20 druggable pockets on the β-cat protein surface, including the specific surfaces for

interaction with TCF and E-cad (Fig. S2*D*). An unbiased computational molecular docking screen of ~1,000 randomly chosen compounds from the initial screening library revealed that iCRT5 and -3 dock preferentially into a TCF-specific pocket lined by Lys435 and Arg469, respectively, on β-cat. The docking is highly specific, with both a good energy score and significant energy gap apparent between the lowest energy docked conformation and other conformations from the same and other pockets (*Materials and Methods* and Fig. 2 *C* and *D*). The docked conformation places a carboxyl (-COOH) group on iCRT5 into a position that mimics interactions mediated by the side chain of Asp16 on TCF4 with K435 on β-cat (Fig. 2*E* and Fig. S3*E*). iCRT3, however, is placed in a position where its -NR group is competent to form a hydrogen bond with Arg469 on β-cat, a residue that is critical for stabilizing β-cat-TCF4 interactions (45) (Fig. 2*F*). The structures of these two compounds are thus highly compatible in terms of molecular shape, electrostatics, and solvation energy, with a pocket on the β-cat protein surface that overlaps the TCF4 binding site. The docking results for iCRT3 and -5 therefore rule out a structural incompatibility between these compounds and the β-cat protein surface and predict their location of binding on the β-cat molecular surface. iCRT14 showed clear shape and energy complementarities with more than one β-cat surface pocket but resulted in a weaker prediction of the exact site of interaction.

Thermal melt analysis. As a preliminary approach to investigating direct binding of iCRT3, -5, and -14 to the β-cat-TCF4 complex, we conducted thermal melt analysis (51) of purified β-cat-TCF4 complexes with and without iCRTs. This method analyzes temperature-dependent denaturation and is sensitive to the binding of small molecules or other protein ligands. As shown in Fig. 2 *G–I*, the addition of iCRT3, -5, and -14 causes a change in the melting temperature of β-cat-TCF4 complexes from the native value of 56.8 °C by as much as 2 °C (Fig. 2 *G–I*). To confirm the validity of this method in studying protein–small molecule interactions, we performed similar thermal melt experiments with the FKBP12 and Rapamycin, which form a well-characterized protein–drug complex (52, 53), and observed a temperature shift of ~1.5 °C in the presence of Rapamycin (Fig. S3*E*).

It is notable that the ability of the iCRTs to disrupt both endogenous and purified β-cat-TCF complexes (Fig. 2 *A* and *B* and Fig. S2*B*) was comparable with the extent of reduction observed between bacterially purified GST-TCF4 and His-β-cat bearing a K435A substitution (Fig. S3 *C* and *D*). These data collectively imply that interfering with a single site of interaction between two proteins, while not disassembling the complex entirely, is nevertheless sufficient to inhibit a cellular function such as transcription. The predictive value of in silico docking studies is corroborated by the cellular evidence that these compounds act at the level of β-cat or downstream. Taken together, our data from biochemical interaction studies, thermal melt analyses, and in silico analyses strongly support the hypothesis of direct binding of candidate iCRTs to β-cat and disruption of β-cat-TCF4 interaction as their mechanism of CRT modulation.

Inhibition of Wnt-Induced Phenotypes in Murine and Human Cancer Cell Lines. For the candidate iCRTs to have therapeutic potential in activated CRT-related diseases, they should be capable of inhibiting a variety of Wnt/CRT-induced cellular phenotypes. We first evaluated their effects in a phenotypic assay using the Wnt responsive mouse mammary epithelial cell line C57MG (Fig. 3). Expression of Wnt genes, such as Wnt1 or Wnt3a, in these cells results in cellular transformation manifested by a change from an epithelium-like morphology to spindle-shaped cells with chord-like actin bundles (54, 55). Treatment with purified Wnt3a protein has a similar effect (56). Addition of candidate iCRTs to such cells in the presence of Wnt3a resulted in significant inhibition of the transformation phenotype (Fig. 3 *B–F*). We quantified these phenotypic changes using an automated imaging system and algorithm that measures the degree of anisotropy of actin fiber alignments within each cell. The anisotropy is the measure of the SD of the angles projected by each of the actin fibers relative to the normal; a low SD reflects an increase in Wnt-induced transformation as the fibers become more aligned. Thus, control non-transformed C57MG cells show a normal bell-shaped distribution of the degree of fiber alignment (Fig. 3*B″*). Wnt3a treatment reduces the degree of anisotropy and results in a skewed distribution of fiber alignment (Fig. 3*C″*). However, this shift is robustly inhibited by treatment with the three candidate iCRTs (Fig. 3 *D″–F″*). In principle, this prevention of transformation could result from either inhibition of CRT or downstream antagonistic effects on the gene products that mediate the morphological change. To investigate this, we used quantitative RT-PCR (qPCR) to examine the mRNA levels of Wnt-1 induced secreted protein 1 (WISP1), a key β-cat target in C57MG cells that is implicated in transformation (57). As shown in Fig. 3*G*, treatment of Wnt3a-induced cells with iCRTs resulted in a significant reduction in WISP1 mRNA levels. This further supports the conclusion that these compounds specifically interfere with β-cat's nuclear signaling activity (CRT), as intended by the design of the primary screen.

Next, we tested the efficacy of iCRTs on MCF7 human breast adenocarcinoma cell lines (a pathologically relevant model for Wnt-induced cell invasion). Activation of Wnt signaling in the otherwise noninvasive MCF-7 cell line leads to acquisition of invasive capacity (58). Recent studies show that this results from β-cat–mediated transcriptional activation of AXN2, which ultimately results in the down-regulation of E-cad expression (58) and concomitant invasion. MCF-7 cells stably transduced with retroviruses expressing HA-tagged S37Aβ-cat were cultured in the presence of iCRT compounds or DMSO and assayed for induction of AXN2 transcription by qRT-PCR and invasiveness in matrigel-coated Boyden chambers. As shown in Fig. 3*H*, S37Aβ-cat-HA strongly induced expression of AXN2 compared with control cells transduced with vector alone. This activation was robustly inhibited by the candidate iCRTs in a dose-dependent manner (Fig. 3*H*). Associated with the S37Aβ-cat-HA–mediated induction of AXN2 in MCF7 cells was a dramatic increase in their capacity to invade Matrigel in transwell assays (Fig. 3*I*). This increased invasive behavior of MCF7-S37Aβ-cat-HA cells was significantly blocked in a dose-dependent fashion by the candidate iCRTs compared with DMSO control (Fig. 3*I*).

Immunostaining for E-cad in MCF7-S37Aβ-cat-HA stable cells revealed a noticeable down-regulation of E-cad expression at the plasma membrane compared with control MCF7 cells (Fig. S4 *F* and *G*). This was also observed in MCF7 cells transfected transiently with S37Aβ-cat and CMV-GFP (Fig. S4 *A* and *B*). Treatment of the stable transfectants with iCRTs inhibited the loss of membranous E-cad as opposed to DMSO, which had no effect (Fig. S4 *G–J*). The block in down-regulation of membranous E-cad in MCF7-S37Aβ-cat-HA cells correlates with the reduced migration of the iCRT-treated cells that we observed in the migration assay (Fig. 3*H* and Fig. S4). Taken together, these data suggest that the candidate small-molecule inhibitors act at the level of CRT and thus, are capable of modulating CRT-induced molecular and morphological changes in a variety of Wnt responsive cells.

iCRTs Are Specifically Cytotoxic to Wnt/CRT-Addicted Colon Cancer Cell Lines. The colon carcinoma cell line HCT-116 offers a pathologically relevant system in which to examine the effects of Wnt signaling inhibitors. HCT-116 cells bear a deletion of codon S45 in β-cat that makes the protein refractory to phosphorylation and degradation. This results in constitutive CRT and Wnt targets such as CycD1 and c-myc are thus overexpressed (59). Importantly, inhibition of Wnt/β-cat signaling in such cancer cells blocks the prosurvival pathway and induces apoptosis (60). To

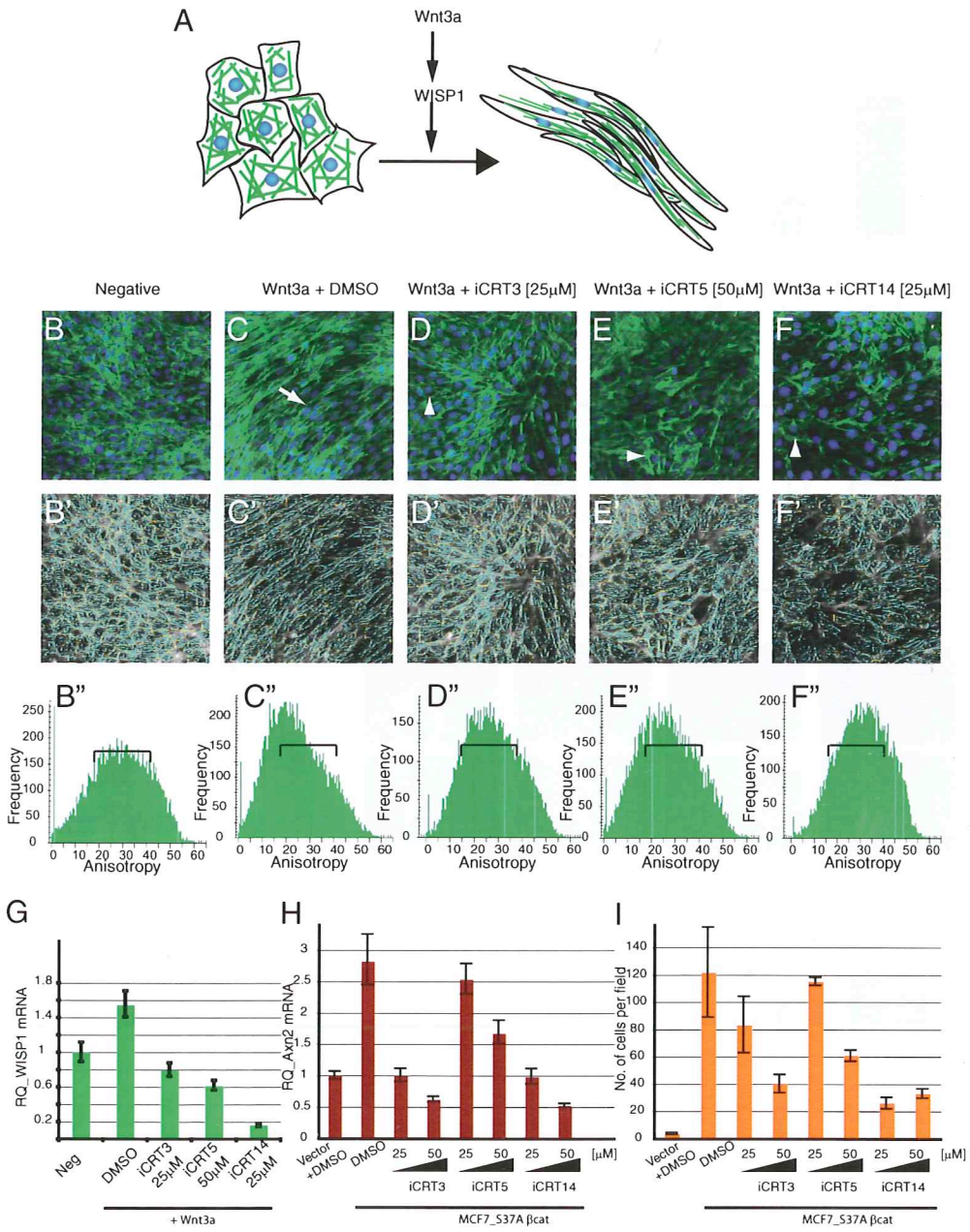

Fig. 3. (*A*) Exposure to Wnt3a causes an evident phenotypic transformation of mouse mammary epithelial cells into long chord-like bundles. (*B–F*) C57MG cells cultured in the presence of Wnt3a and compounds and/or DMSO stained with DAPI (blue) and FITC-conjugated phalloidin (green) for quantitative high-content image analysis. Candidate compounds inhibit (arrowhead in *D–F*) the acquisition of the chord-like phenotype seen in DMSO+Wnt3a-treated cells (arrow in *C*). The algorithm used to quantify this phenotypic transformation identifies intracellular actin fibers (blue overlay in *B′–F′*) and calculates the anisotropy of the actin fiber alignment within each individual cell (yellow mask outline in *B′–F′*). (*B″–F″*) Histogram plot of anisotropy of fiber alignment in cell populations ($n \geq 8{,}000$) treated with individual candidate compounds shows normal distribution in controls; normal peak maxima is highlighted by the square bracket (*B″*). Treatment with Wnt3a+DMSO results in a skewed distribution of anisotropy (*C″*), which is rescued by treatment with candidate compounds (*D″–F″*). (Scale bar: 5 μm.) (*G*) Quantification of the β-cat target gene, WISP1, in response to treatment with candidate compounds. Error bars show range of variation from mean. (*H*) MCF7-S37Aβ-cat-HA cells show increased accumulation of Axn2 mRNA compared with control cells, which is inhibited by treatment with candidate compounds. (*I*) MCF7-S37Aβ-cat-HA cells exhibit invasive potential as assayed by the Boyden chamber invasion assay. Treatment with candidate compounds results in a marked decrease in the number of invading cells.

test the inhibitory effect of candidate iCRTs on the transcription of endogenous Wnt/β-cat target genes in HCT116 cells, we performed qRT-PCR assays for CYCD1 and AXN2. These are well-characterized targets of CRT, and their expression was reduced in response to transfection with siRNA against β-cat (Fig. 4*A*). We also observed a significant reduction in AXN2 and CYCD1 mRNA in HCT116 cells treated with iCRT3, -5, and -14 (Fig. 4*B*). Importantly, the extent of inhibition by iCRTs was similar to that observed on siRNA-mediated knockdown of β-cat (Figs. 4 *A* and *B*). Lysates prepared from iCRT-treated cells showed a corresponding reduction in CYCD1 protein levels compared with DMSO-treated controls (Fig. 4*C*). Similar results were also obtained with C-MYC, another well-documented Wnt target (Fig. S3 *A* and *B*).

We next analyzed the iCRT-treated HCT116 cells by flow cytometry and observed a marked cell cycle arrest in the G0/G1

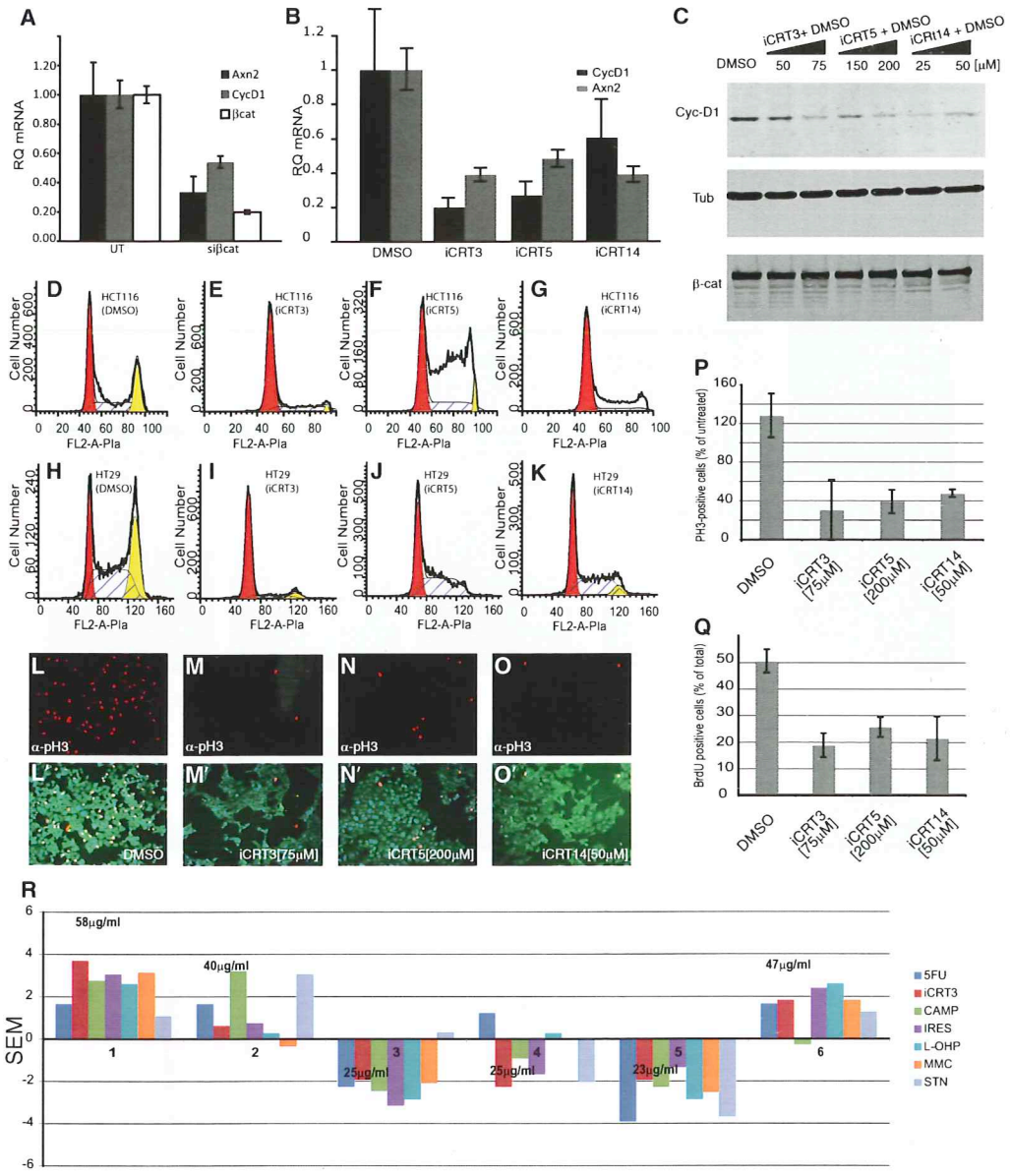

Fig. 4. (*A*) HCT116 cells transfected with siβ-cat show reduced accumulation of Axn2 and CycD1 mRNA, thereby suggesting β-cat–directed transcription of these targets. (*B*) Inhibition of Axn2, cyc-D1 transcription in response to treatment of HCT116 cells with 50 μM iCRT3 (75 μM for cyc-D1), 50 μM iCRT5 (200 μM for cyc-D1), and 50 μM iCRT14. (*A* and *C*) Western blots showing inhibition of β-cat target Cyc-D1 accumulation in HCT116 cells in response to varying concentrations of candidate compounds. iCRTs have no effect on the accumulation or stability of β-cat. Treatment of HCT116 (*D–G*) and HT29 (*H–K*) cell lines with 75 μM iCRT3 (*E* and *I*), 200 μM iCRT5 (*F* and *J*), and 50 μM iCRT14 (*G* and *K*) causes a clear cell cycle arrest as shown by flow cytometry. DMSO has no effect on the cell cycle profile of HCT116 (*D*) and HT29 (*H*) cells. Red peaks depict cells in G0/G1; yellow depicts G2/M. (*L–P* and *L′–O′*) Inhibition of HCT116 proliferation is confirmed by reduction in the number of PH3-positive cells when cultured in the presence of candidate compounds at the indicated concentrations. (*Q*) Cell cycle arrest caused by compound treatment is also reflected in the reduced number of BrdU-positive cells. (*R*) Positive or negative SEMs of IC_{50} values (shown) of iCRT3 compared with that of other drugs show differential sensitivity of colon cancer biopsies from six individual patients to therapeutic agents. Three patient samples show high sensitivity to iCRT3. IC_{50} values in milligrams per milliliter for iCRT3 in each of the samples tested are depicted above in the graph. 5FU, fluorouracil; CAMP, camptosar; IRES, IRESSA; L-OHP, oxaliplatin; MMC, mitomycin-C; STN, sutent. IC_{50} values of iCRT3 in individual colon cancer samples are depicted in milligrams per milliliter.

phase, consistent with the reduction in CYCD1 expression (Fig. 4 *D–G*). Effects of iCRTs were also tested on the colon cancer cell line HT29, which bears a mutation in the APC gene resulting in abnormally high levels of transcriptionally active β-cat (61). Compound-treated HT29 cells (Fig. 4 *H–K*) showed strong G0/G1 arrest, as observed in HCT116. This cell cycle arrest in the presence of iCRTs correlated with a drastic reduction in both the number of cells staining positive for phospho-histone3 (Fig. 4 *L–P* and *L′–O′*) and the number of cells that incorporated BrdU (Fig. 4*Q*). The iCRT effects on cell growth and proliferation observed in the HCT116 and HT29 cell lines were not seen in HEK293, C57MG, MCF7, or *Drosophila* Cl8 cells after overnight exposure to the compounds. Thus, of the cell lines tested, growth inhibition was only observed in those that exhibit constitutively elevated levels of CRT and are thought to be dependent on sustained Wnt/CRT activity for their survival. Our data suggest that this property may allow the compounds to be used for specific therapeutic purposes to induce apoptosis of Wnt-dependent can-

cer cells/tumor tissue without affecting growth and proliferation of normal healthy cells.

Validation of Candidate Compounds in Primary Tumor Samples and Mouse Xenograft Models of HCT116 and HT29 Cells. ***Effect on colon cancer patient biopsies.*** Primary human colon cancer specimens obtained from patients were used to assess the effects of iCRT3 in human cancer. Six individual tissue samples received under IRB-approved protocol (*SI Materials and Methods*) were disaggregated into microspheroids, each comprised of 50–70 cells and cultured in the presence of varying concentrations of iCRT3 or commonly used chemotherpeutics such as fluorouracil (5-FU), camptosar (CAMP), oxaliplatin (L-OHP), IRESSA (IRES), mitomycin-C (MMC), and sutent (STN). Two assay endpoints, the delayed loss of membrane integrity and the ATP content by luciferin-luciferase, were used to assess drug-induced cytotoxicity and determine the sample-specific IC_{50} for each of the drugs, as previously described (62). iCRT3 at concentration ranges of 6.25–100 μg/mL showed cytotoxicity in human primary culture specimens with an average IC_{50} of 36 μg/mL. Strikingly, this is in a range comparable with that for the other drugs tested: 5FU = 77 μg/mL; CAMP = 53 μg/mL; IRESSA = 10.7 μg/mL; L-OHP = 6.7 μg/mL; MMC = 1.7 μg/mL; STN = 7.3 μg/mL. The response of different patient samples to the drugs tested, as judged by the SEM of individual IC_{50} values, reveals differential sensitivity of each of the patient samples to iCRT3 as well as to the other drugs (Fig. 4*R*). This underscores the fact that response to particular therapeutic agents depends on several factors such as progress of disease and genetic variation. Nonetheless, the observation that three patient samples were highly sensitive to iCRT3, with IC_{50} values comparable with those of well-established drugs, is remarkable in that this compound was identified in a primary screen and has not undergone any chemical modifications. This, coupled with the fact that three patient samples were insensitive to iCRT3, suggests that the compound is not a general cytotoxin and thus offers significant potential for its further improvement as a pharmacological agent.

HCT116 and HT29 xenografts. Due to limited commercial availability of the candidate iCRTs and their structural as well as functional similarities, we selected iCRT14 for in vivo testing. We chose the HCT116 and HT29 xenograft models: both of these result in rapidly proliferating tumors when implanted s.c. in athymic nude mice. After measurable tumors of at least 80–120 mm^3 volume were established, the animals were administered iCRT14 (dissolved in DMSO) at a concentration of 50 mg/kg. The compound was administered by i.p. injection three times a week for 3 wk. Immunostaining of xenograft sections after different time periods revealed a marked decrease in CycD1 compared with DMSO-treated controls (Fig. S5 *A* and *B*). This coincided with reduced proliferation of the tumors, reflected by fewer numbers of cells staining positive for phospho-histone3 in drug-treated tumors (Fig. S5 *C* and *D*); similar results were seen in HT29 xenografts (Fig. S5 *E–H*). Furthermore, these effects were correlated with a marked reduction (~50%) in the initial growth rate of tumors within the first 3 wk (~day 19) of compound administration (Fig. S5 *I* and *J*). After day 19, however, the rate of tumor growth was comparable with that of DMSO-treated control. Administration of a lower concentration of compound (20 mg/kg) by minipump also resulted in identical effects in HCT116 xenografts (Fig. S5*I*). Importantly, throughout the course of the study, the mice did not display any signs of systemic toxicity or weight loss that would indicate off-target or nonspecific effects.

It is possible that the tumor growth results above could have been influenced by a slow rate of angiogenesis relative to the rapid growth rate of the tumor mass in such xenografts (63). Thus, cells that are far removed from the growing vasculature might continue to proliferate at rates comparable with DMSO-treated controls. Also, the iCRT-treated tumors exhibited a marked increase in necrosis compared with DMSO controls, and the volume of necrotic tissue may contribute to the gross measurement of external tumor volume. It is, therefore, possible that the modest reduction in compound-treated xenograft volume is partially influenced by the reduced capacity for clearance of necrotic tissue in immunodeficient mice. Additionally, the compound may be metabolized rapidly in vivo, thus reducing its bioavailability. Nonetheless the consistent, albeit modest, reduction of tumor xenograft growth that we observed is particularly striking given that this is an unmodified compound from a primary screen.

Discussion

A key feature in early drug discovery is the design and implementation of an efficient and reliable screening strategy. We anticipate that the results from our study will encourage the incorporation of similar RNAi-based targeted screening methodologies for identification of specific small-molecule modulators of other cell signaling pathways in a physiological context.

Although protein–protein interaction surfaces have traditionally been challenging targets for drug development, there is increasing evidence from several recent studies that such interactions can indeed be targeted by small molecules that compete for hotspots of interactions on the surface of target proteins (64). The data that we present here corroborate the previously postulated notion (20) that specific interference of the protein interaction surfaces between endogenous β-cat and TCF (and perhaps other components of the CRT complex) is not only feasible but also a viable strategy that can be used to modulate nuclear functions of β-cat in a cellular context. Importantly, the iCRTs identified in this study represent a significant increase in efficacy compared with a previously known inhibitor, such as Calphostin C (20), that was shown to use a similar inhibitory mechanism on Wnt responsive reporter activity (Fig. S6). Although our results show that the candidate iCRTs can directly influence the interaction between β-cat and its transcriptional partner TCF4, confirmation of these specific interactions and their structural details must wait for the solving of crystal structures of β-cat in complex with the candidate small molecules, which is currently underway. Nonetheless, the results from our molecular docking studies provide preliminary testable hypotheses in this regard. Future studies will also test the possibility of whether some of the candidate iCRTs influence pair-wise interactions between the other core components of the β-catenin transcriptional complex, such as Bcl9 and Pygo.

We envision that small molecules identified in screens such as those reported here can serve as prototypes for the development of antitumor drugs targeting CRT programs in different cancers. Although there is a clear need for improving the efficacy/potency of the lead compounds that we have identified in this initial study, we believe that our lead iCRTs (iCRT3, -5, and -14) satisfy a required profile for further investigation as inhibitors of tumor establishment and/or metastasis in vivo. Such a profile consists of five components: (*i*) an IC_{50} in the nanomolar to micromolar range in assays of pathway activity using luciferase-based Wnt reporters; (*ii*) low complexity compounds with molecular weights in the range of <300–400 Da; (*iii*) the ability to inhibit direct interactions of β-cat with its cognate transcription factors, such as TCF4, without indiscriminately affecting its interaction with protein partners at the plasma membrane, such as E-cad and α-cat, and/or the ability to disrupt binding of TCF/LEF transcription factors onto their cognate DNA binding sites (iCRT14 in Fig. 2 *C* and *D*); (*iv*) the ability to inhibit transcription of known downstream target genes of β-cat, such as WISP-1, Axin-2, CycD1, and c-myc, in variety of cell types without affecting β-cat protein expression levels; (*v*) the ability to inhibit a variety of Wnt responsive phenotypes, such as cellular transformation in C57MG cells, cell invasion in MCF7 cells, and cell growth and proliferation in Wnt/β-cat–addicted cancer cells, such as HCT116 and HT29; and (*vi*) the modest but consistent potency

in inhibiting CRT in an in vivo xenograft context while not causing any significant systemic toxicity. Most importantly, our studies of the cytotoxic effects of iCRTs in human colon cancer samples indicate an efficacy comparable with that of FDA-approved cancer drugs such as 5 FU. These iCRTs are therefore attractive lead compounds that can now be further developed for therapeutic intervention in Wnt-associated cancers.

In conclusion, our targeted screening methodology resulted in the identification of small molecules that can modify Wnt signaling activity at a specific step in the signal transduction cascade. Similar RNAi-based integrated screening technology should be widely applicable to a variety of other signaling pathways implicated in human development and disease.

Materials and Methods

Primary Screen. The primary screen was conducted in a 384-well format, for which 40×10^3 *Drosophila* Cl8 cells were transfected with 50 ng each dTF12-LF Wg signaling reporter and PolIII-RL normalization reporter as well as 100 ng dAxin dsRNA using Effectene transfection reagent (Qiagen). After 4 d of incubation to ensure complete knockdown of Axin, small-molecule compounds from the indicated libraries were added to a final concentration of 9 ng/μL in a final volume of 60 μL. After incubation for ~16 h, normalized luciferase activity was measured using the Dual-Glo luciferase system (Promega). The *Z* factor, which reflects the fidelity and efficacy of the screening paradigm, was calculated as follows: Z factor = $1 - [3(\sigma p - \sigma n)/|\mu p - \mu n|]$, where σp = SD of positive control, σn = SD of negative control, μp = mean of positive control, and μn = mean of negative control.

Constructs. SuperTopFlash (STF16; 16×) and 12XdTOP (dTF12) constructs have been previously described in DasGupta et al. (34). HA-tagged S37Aβ-cat was prepared by amplifying S37Aβ-cat with specific primer pairs, wherein the HA tag sequence was incorporated into the reverse primer. S37Aβ-cat-HA was cloned into the BamH1/Sal1 sites in pBabe for generation of retroviral transduction construct.

Cell Lines. HCT116 and HEK293T/17 cell lines were obtained from ATCC. The MCF-7 cell line was a gift from Michael Garabedian's laboratory (New York University School of Medicine, New York, NY). The C57MG cell line was a gift from Pamela Cowin's laboratory (New York University School of Medicine, New York, NY). HCT116 cells were cultured in McCoy's 5A medium supplemented with 10% FBS. MCF7, C57MG, Rat2, and HEK 293/T17 cells were cultured in DMEM supplemented with 10% FBS. *Drosophila* Cl8 cells were obtained from *Drosophila* RNAi Screening Center (DRSC), Harvard University, Cambridge, MA, and cultured in Shields and Sang M3 Insect Media supplemented with 0.0125 IU/mL insulin (16634; Sigma-Aldrich), 2.5% fly extract, and 2% FBS at 23 °C. Detailed protocols for the cell-based assays are described in *SI Materials and Methods*.

CoIP and Target Accumulation Assays. Standard techniques were used for coIP assays between β-cat and TCF-4 in HEK293T/17 cells. Detailed protocol described in *SI Materials and Methods*.

qRT-PCR Analysis. Target accumulation validations were performed by qPCR after treatment with the lead compounds. Briefly, cells were treated with specified concentrations of compounds for 1 d (MCF7 cells and HCT116 cells) or 5 d (C57MG cells) and lysed in 50 μL cell lysis buffer (AM8723; Ambion) at 75 °C for 10 min. First-strand cDNA was prepared using a High-Capacity Reverse Transcription Kit (Applied Biosystems) as per the manufacturer's instructions. Real-time qPCR was carried out for Axn2, E-cad, CycD1, c-Myc, and GAPDH2 (endogenous control) using prevalidated gene-specific primer pairs from Qiagen and the SYBR green PCR master mix from Applied Biosystems. Data analysis was performed using the MxPro-Mx3005P system from Stratagene using the ddCt method.

Thermal Stability Analysis. Purified β-cat-His and TCF4-*N*-GST were mixed in a 1:2 molar ratio in 1× PBS at room temperature in the presence of various concentrations of iCRTs and 0.5× SYPRO Orange (S6651; Invitrogen). Samples were heated in 96-well plates using a LightCycler 480 System (Roche) from 20 °C to 95 °C at a ramp rate of 0.06 °C per s. Fluorescence readings were acquired at 0.1-s intervals during the heating phase. Melting temperatures were calculated by plotting negative derivates of fluorescence intensity reading against temperature. Inflection point on the negative derivative curve is considered the melting temperature (Tm).

ACKNOWLEDGMENTS. We thank Carolyn Shamu from the ICCB–Longwood Screening Facility where the primary screen was performed. We would also like to acknowledge Sarah Burroughs for help with Array Scan Image analysis algorithms; Chi-Yun and Shauna Katz (New York University RNAi Facility) for help with various assays; members of the R.D. and Bach laboratories for suggestions on experiments; Srikala Raghavan and Aditi Bandopadhyay for help with viral transduction experiments and mouse keratinocytes; Dr. Cara Gottardi for the TCF-VP16 and ΔNlef-β-cat constructs; and Dr. Susan Logan and Eugine Lee for help with TCF-VP16 transfections. We also thank Bernard Mathey-Prevot, Srikala Raghavan, and Brian Dynlacht for critical reading of the manuscript. C57MG cells were a gift from Pamela Cowin. This work was supported by National Institutes of Health Grants 1DP2OD002867-01 (to T.C.), 5R01CA123238 (to A.B.), and 1R21HD057525-01 (to R.D.), Department of Defense Concept Award W81XWH-07-1-0541 (to R.D.), and a Kimmel Stem Cell Postdoctoral fellowship (to F.C.G.).

1. Miller JR, Hocking AM, Brown JD, Moon RT (1999) Mechanism and function of signal transduction by the Wnt/beta-catenin and Wnt/Ca2+ pathways. *Oncogene* 18:7860–7872.
2. Polakis P (2000) Wnt signaling and cancer. *Genes Dev* 14:1837–1851.
3. Wodarz A, Nusse R (1998) Mechanisms of Wnt signaling in development. *Annu Rev Cell Dev Biol* 14:59–88.
4. Miyoshi K, Hennighausen L (2003) Beta-catenin: A transforming actor on many stages. *Breast Cancer Res* 5:63–68.
5. Miyoshi K, et al. (2002) Activation of different Wnt/beta-catenin signaling components in mammary epithelium induces transdifferentiation and the formation of pilar tumors. *Oncogene* 21:5548–5556.
6. Moon RT, Kohn AD, De Ferrari GV, Kaykas A (2004) WNT and beta-catenin signalling: Diseases and therapies. *Nat Rev Genet* 5:691–701.
7. Hart M, et al. (1999) The F-box protein beta-TrCP associates with phosphorylated beta-catenin and regulates its activity in the cell. *Curr Biol* 9:207–210.
8. Marikawa Y, Elinson RP (1998) beta-TrCP is a negative regulator of Wnt/beta-catenin signaling pathway and dorsal axis formation in Xenopus embryos. *Mech Dev* 77: 75–80.
9. Yanagawa S, Lee JS, Matsuda Y, Ishimoto A (2000) Biochemical characterization of the Drosophila axin protein. *FEBS Lett* 474:189–194.
10. Yanagawa S, et al. (2002) Casein kinase I phosphorylates the Armadillo protein and induces its degradation in Drosophila. *EMBO J* 21:1733–1742.
11. Nusse R (1999) WNT targets. Repression and activation. *Trends Genet* 15:1–3.
12. Staal FJ, Clevers H (2000) Tcf/Lef transcription factors during T-cell development: Unique and overlapping functions. *Hematol J* 1:3–6.
13. Schweizer L, Nellen D, Basler K (2003) Requirement for Pangolin/dTCF in Drosophila Wingless signaling. *Proc Natl Acad Sci USA* 100:5846–5851.
14. Furlong MT, Morin PJ (2000) Rare activation of the TCF/beta-catenin pathway in ovarian cancer. *Gynecol Oncol* 77:97–104.
15. Giles RH, van Es JH, Clevers H (2003) Caught up in a Wnt storm: Wnt signaling in cancer. *Biochim Biophys Acta* 1653:1–24.
16. Segditsas S, Tomlinson I (2006) Colorectal cancer and genetic alterations in the Wnt pathway. *Oncogene* 25:7531–7537.
17. Senda T, Iizuka-Kogo A, Onouchi T, Shimomura A (2007) Adenomatous polyposis coli (APC) plays multiple roles in the intestinal and colorectal epithelia. *Med Mol Morphol* 40:68–81.
18. Park JY, et al. (2005) Mutations of beta-catenin and AXIN I genes are a late event in human hepatocellular carcinogenesis. *Liver Int* 25:70–76.
19. Satoh S, et al. (2000) AXIN1 mutations in hepatocellular carcinomas, and growth suppression in cancer cells by virus-mediated transfer of AXIN1. *Nat Genet* 24: 245–250.
20. Lepourcelet M, et al. (2004) Small-molecule antagonists of the oncogenic Tcf/beta-catenin protein complex. *Cancer Cell* 5:91–102.
21. Chen B, et al. (2009) Small molecule-mediated disruption of Wnt-dependent signaling in tissue regeneration and cancer. *Nat Chem Biol* 5:100–107.
22. Huang SM, et al. (2009) Tankyrase inhibition stabilizes axin and antagonizes Wnt signalling. *Nature* 461:614–620.
23. Vo N, Goodman RH (2001) CREB-binding protein and p300 in transcriptional regulation. *J Biol Chem* 276:13505–13508.
24. Thorne CA, et al. (2010) Small-molecule inhibition of Wnt signaling through activation of casein kinase 1α. *Nat Chem Biol* 6:829–836.
25. Birchmeier W, Behrens J (1994) Cadherin expression in carcinomas: Role in the formation of cell junctions and the prevention of invasiveness. *Biochim Biophys Acta* 1198:11–26.
26. Näthke I (2006) Cytoskeleton out of the cupboard: Colon cancer and cytoskeletal changes induced by loss of APC. *Nat Rev Cancer* 6:967–974.
27. Chen M, et al. (2009) The anti-helminthic niclosamide inhibits Wnt/Frizzled1 signaling. *Biochemistry* 48:10267–10274.
28. Shan J, Shi DL, Wang J, Zheng J (2005) Identification of a specific inhibitor of the dishevelled PDZ domain. *Biochemistry* 44:15495–15503.
29. Lum L, et al. (2003) Identification of Hedgehog pathway components by RNAi in Drosophila cultured cells. *Science* 299:2039–2045.

30. Cox RT, Kirkpatrick C, Peifer M (1996) Armadillo is required for adherens junction assembly, cell polarity, and morphogenesis during Drosophila embryogenesis. *J Cell Biol* 134:133–148.
31. Pai LM, et al. (1996) Drosophila alpha-catenin and E-cadherin bind to distinct regions of Drosophila Armadillo. *J Biol Chem* 271:32411–32420.
32. Peifer M, Orsulic S, Pai LM, Loureiro J (1993) A model system for cell adhesion and signal transduction in Drosophila. *Dev Suppl* 163–176.
33. Hülsken J, Birchmeier W, Behrens J (1994) E-cadherin and APC compete for the interaction with beta-catenin and the cytoskeleton. *J Cell Biol* 127:2061–2069.
34. DasGupta R, Kaykas A, Moon RT, Perrimon N (2005) Functional genomic analysis of the Wnt-wingless signaling pathway. *Science* 308:826–833.
35. Hoffmans R, Basler K (2007) BCL9-2 binds Arm/beta-catenin in a Tyr142-independent manner and requires Pygopus for its function in Wg/Wnt signaling. *Mech Dev* 124: 59–67.
36. Städeli R, Basler K (2005) Dissecting nuclear Wingless signalling: Recruitment of the transcriptional co-activator Pygopus by a chain of adaptor proteins. *Mech Dev* 122: 1171–1182.
37. Hendriksen J, et al. (2005) RanBP3 enhances nuclear export of active (beta)-catenin independently of CRM1. *J Cell Biol* 171:785–797.
38. Wang PS, et al. (2009) Thiazolidinediones downregulate Wnt/beta-catenin signaling via multiple mechanisms in breast cancer cells. *J Surg Res* 153:210–216.
39. Wei S, et al. (2007) Thiazolidinediones modulate the expression of beta-catenin and other cell-cycle regulatory proteins by targeting the F-box proteins of Skp1-Cul1-F-box protein E3 ubiquitin ligase independently of peroxisome proliferator-activated receptor gamma. *Mol Pharmacol* 72:725–733.
40. Sadot E, et al. (2002) Regulation of S33/S37 phosphorylated beta-catenin in normal and transformed cells. *J Cell Sci* 115:2771–2780.
41. González-Sancho JM, Brennan KR, Castelo-Soccio LA, Brown AM (2004) Wnt proteins induce dishevelled phosphorylation via an LRP5/6-independent mechanism, irrespective of their ability to stabilize beta-catenin. *Mol Cell Biol* 24:4757–4768.
42. Nybakken K, Vokes SA, Lin TY, McMahon AP, Perrimon N (2005) A genome-wide RNA interference screen in Drosophila melanogaster cells for new components of the Hh signaling pathway. *Nat Genet* 37:1323–1332.
43. Miravet S, et al. (2002) The transcriptional factor Tcf-4 contains different binding sites for beta-catenin and plakoglobin. *J Biol Chem* 277:1884–1891.
44. Omer CA, Miller PJ, Diehl RE, Kral AM (1999) Identification of Tcf4 residues involved in high-affinity beta-catenin binding. *Biochem Biophys Res Commun* 256:584–590.
45. von Kries JP, et al. (2000) Hot spots in beta-catenin for interactions with LEF-1, conductin and APC. *Nat Struct Biol* 7:800–807.
46. Fasolini M, et al. (2003) Hot spots in Tcf4 for the interaction with beta-catenin. *J Biol Chem* 278:21092–21098.
47. Huber AH, Weis WI (2001) The structure of the beta-catenin/E-cadherin complex and the molecular basis of diverse ligand recognition by beta-catenin. *Cell* 105:391–402.
48. Graham TA, Weaver C, Mao F, Kimelman D, Xu W (2000) Crystal structure of a beta-catenin/Tcf complex. *Cell* 103:885–896.
49. Eklof Spink K, Fridman SG, Weis WI (2001) Molecular mechanisms of beta-catenin recognition by adenomatous polyposis coli revealed by the structure of an APC-beta-catenin complex. *EMBO J* 20:6203–6212.
50. Liu J, Wang H, Zuo Y, Farmer SR (2006) Functional interaction between peroxisome proliferator-activated receptor gamma and beta-catenin. *Mol Cell Biol* 26:5827–5837.
51. Lo MC, et al. (2004) Evaluation of fluorescence-based thermal shift assays for hit identification in drug discovery. *Anal Biochem* 332:153–159.
52. Bierer BE, et al. (1990) Two distinct signal transmission pathways in T lymphocytes are inhibited by complexes formed between an immunophilin and either FK506 or rapamycin. *Proc Natl Acad Sci USA* 87:9231–9235.
53. Bierer BE, Somers PK, Wandless TJ, Burakoff SJ, Schreiber SL (1990) Probing immunosuppressant action with a nonnatural immunophilin ligand. *Science* 250: 556–559.
54. Brown AM, Wildin RS, Prendergast TJ, Varmus HE (1986) A retrovirus vector expressing the putative mammary oncogene int-1 causes partial transformation of a mammary epithelial cell line. *Cell* 46:1001–1009.
55. Shimizu H, et al. (1997) Transformation by Wnt family proteins correlates with regulation of beta-catenin. *Cell Growth Differ* 8:1349–1358.
56. Willert K, et al. (2003) Wnt proteins are lipid-modified and can act as stem cell growth factors. *Nature* 423:448–452.
57. Xu L, Corcoran RB, Welsh JW, Pennica D, Levine AJ (2000) WISP-1 is a Wnt-1- and beta-catenin responsive oncogene. *Genes Dev* 14:585–595.
58. Yook JI, et al. (2006) A Wnt-Axin2-GSK3beta cascade regulates Snail1 activity in breast cancer cells. *Nat Cell Biol* 8:1398–1406.
59. Behrens J (2000) Control of beta-catenin signaling in tumor development. *Ann N Y Acad Sci* 910:21–33.
60. He B, et al. (2005) Blockade of Wnt-1 signaling induces apoptosis in human colorectal cancer cells containing downstream mutations. *Oncogene* 24:3054–3058.
61. Morin PJ, Vogelstein B, Kinzler KW (1996) Apoptosis and APC in colorectal tumorigenesis. *Proc Natl Acad Sci USA* 93:7950–7954.
62. Nagourney RA (2006) Ex vivo programmed cell death and the prediction of response to chemotherapy. *Curr Treat Options Oncol* 7:103–110.
63. Huxham LA, Kyle AH, Baker JH, Nykilchuk LK, Minchinton AI (2004) Microregional effects of gemcitabine in HCT-116 xenografts. *Cancer Res* 64:6537–6541.
64. Bowman AL, Nikolovska-Coleska Z, Zhong H, Wang S, Carlson HA (2007) Small molecule inhibitors of the MDM2-p53 interaction discovered by ensemble-based receptor models. *J Am Chem Soc* 129:12809–12814.